PHOTONIC BAND STRUCTURE

E. Yablonovitch

We employ the concepts of band theory to describe the behavior of electromagnetic waves in three dimensionally periodic face–centered–cubic (fcc) dielectric structures. This can produce a "photonic band gap" in which optical modes, spontaneous emission, and zero point fluctuations are all absent. In the course of a broad experimental survey, we have found that most fcc dielectric structures have "semi–metallic" band structure. Nevertheless, we have identified one particular dielectric "crystal" which actually has a "photonic band gap". This dielectric structure, consisting of 86% empty space, requires a refractive index contrast greater than 3 to 1, which happens to be readily obtainable in semiconductor materials.

1. INTRODUCTION

By analogy to electron waves in a crystal, light waves in a three dimensionally periodic dielectric structure should be described by band theory. Recently, the idea of photonic band structure [1,2] has been introduced. This means that the concepts of reciprocal space, Brillouin zones, dispersion relations, Bloch wave functions, van Hove singularities, etc., must now be applied to electromagnetic waves. If the depth of refractive index modulation is sufficient, then a "photonic band gap" could open up. This is an energy band in which optical modes, spontaneous emission, and zero point fluctuations are all absent.

It is interesting that the most natural real space structure for the optical medium is face–centered–cubic (fcc), which also happens to be the most famous atomic arrangement in crystals. The contrasts between electronic and photonic band structure are striking:

(i) The underlying dispersion relation for electrons is parabolic, while that for photons is linear.

(ii) The angular momentum of electrons is 1/2, but the scalar wave approximation is frequently made; in contrast, photons have spin 1 and the vector wave character plays a major role in the band structure.

(iii) Band theory of electrons is only an approximation due to electron–electron repulsion, while photonic band theory is essentially exact since photon interactions are negligible.

The possible applications of such a "photonic band gap" are quite tantalizing. In addition to quantum electronic applications, such as spontaneous emission inhibition [1], there have also been proposals [2,3] to study mobility edges and Anderson localization within such a forbidden gap. Furthermore, Kurizki *et al.* [4] have shown that atomic and molecular physics is profoundly modified in a volume

W. van Haeringen and D. Lenstra (eds.), Analogies in Optics and Micro Electronics, 117–133.

of space in which "vacuum fluctuations" are absent. In particular, the interatomic potential of homonuclear diatomic molecules, as well as many other atomic physical properties are severely modified in such a spatial region.

Since we are only at the threshold of such research, we have elected to do our initial experimental work at microwave frequencies, where the periodic dielectric structures can be fabricated by conventional machine tools. Furthermore, this has enabled us to use sophisticated microwave homodyne detection techniques to measure the phase and amplitude of the electromagnetic Bloch wave functions propagating through the "photonic crystal".

Earlier work [1,2] had indicated that it was desirable for the Brillouin Zone in reciprocal space to be as near to spherical as possible. Among possible 3–dimensional periodic structures, this had suggested that face–centered–cubic (fcc) dielectric geometry would be optimal for achieving a "photonic band gap". The lowest order Brillouin Zone for the fcc structure happens to be nearer to spherical than the Brillouin Zone of any other common crystal structure. In the absence of any further theoretical guidance, we adopted an empirical, Edisonian approach. Literally, we used the cut–and–try method. Dozens of face–centered–cubic structures were painstakingly machined out of low–loss dielectric materials. These structures, which might be called "crystals", were roughly cube–shaped and contained up to ~ 8000 "atoms". In some cases the "atoms" were dielectric spheres, in other cases the "atoms" were spherical cavities filled with air ("spherical air–atoms"), the interstitial space consisting of dielectric material. The atomic volume filling fraction was varied from 11% to 86%. Refractive index contrast was varied between 1.6 to 1 and 3.5 to 1. The propagation of electromagnetic waves through these structures was then carefully investigated. This tedious cut–and–try approach was very time consuming, but it helped to ensure that no possibilities were overlooked.

The main conclusion of this paper is that a photonic band gap can indeed be achieved in 3–dimensional dielectric structures, but it requires an index contrast nearly 3.5 to 1. The early predictions had been much more optimistic, anticipating a gap opening up at index contrast 1.21 to 1 in one case [1] and 1.46 to 1 in the other [2]. In the experiments, all the test structures except one turned out to be "semi–metals" and only one particular geometry having index contrast 3.5 to 1 gave rise to a "semiconductor" with a true photonic band gap. In semi–metals, the valence band in one section of the Brillouin Zone has an energy overlap with the conduction band in a different section of the Brillouin Zone. A true bandgap, as in a semiconductor, requires a forbidden band of energies *irrespective of the propagation direction* in reciprocal space.

Fortunately, crystalline Silicon and other semiconductors, are excellent infrared optical materials, providing refractive indices ~3.5. Therefore the optimal structure we have found in the microwave experiments can be scaled down in size to provide a photonic band gap in the near infrared.

2. EXPERIMENT

The investigations employed the experimental arrangement shown in Fig.1. A monopole antenna (a 6 mm pin above a ground plane) launches a spherical wave down a long anechoic chamber built of microwave absorbing pads. The wave–front becomes approximately planar by the time it reaches the fcc dielectric structure at the opposite end of the chamber. (Henceforth the fcc dielectric structure will be called the "crystal"). Only the plane wave passing directly through the crystal can

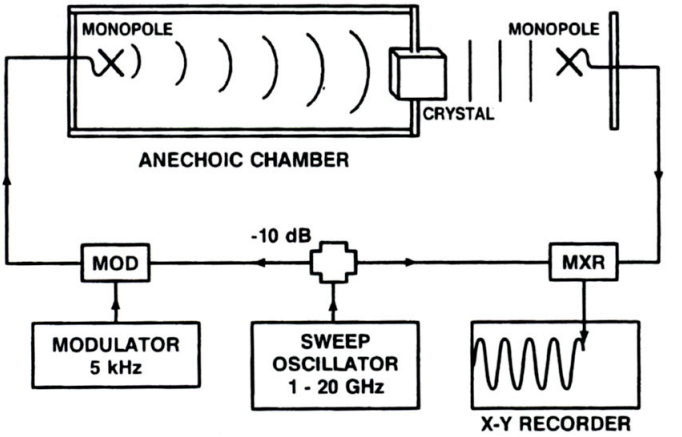

Fig.1 A sweep oscillator feeds a 10dB splitter. Part of the signal is modulated (MOD) and then propagated as a plane wave through a face–centered–cubic dielectric crystal. The other part of the signal is used as local oscillator for the mixer (MXR) to measure the amplitude change and phase shift in the crystal. Between the mixer and the X–Y–recorder is a lock–in amplifier (not shown)

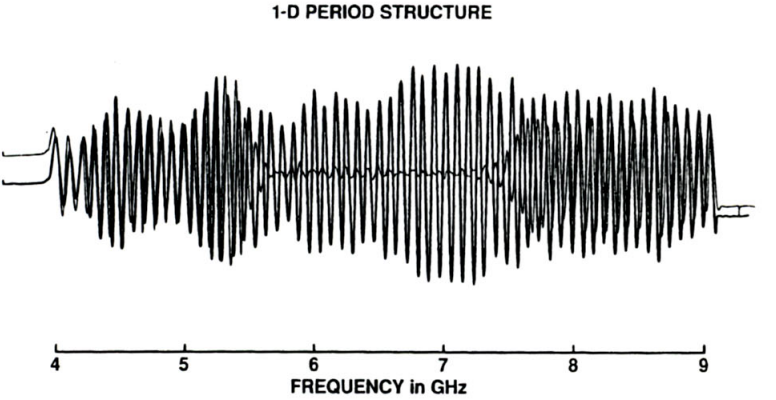

Fig.2 The interference pattern produced when a microwave signal being transmitted between antennas interferes with a local oscillator wave. The heavy line is a reference fringe pattern for the case of transmission through an empty space. The envelope fluctuations are due to variations in antenna efficiency. The lighter line is for transmission through 9 polystyrene plates spaced at one–quarter wavelength. A bandgap opens up between 5.5 GHz and 7.5 GHz. Furthermore, on either side of the bandgap there is $\sim 180^{\circ}$ phase shift.

be seen by the receiving monopole. A microwave oscillator feeds the homodyne detection system with a frequency sweep from 1 to 20 GHz. This home–built system resembles an optical Mach–Zender interferometer. (Alternatively, an HP–8510 Network Analyzer, was also used to perform the amplitude and phase measurements.) The X–Y recorder plots the interference pattern as a function of microwave frequency.

An example of such a series of interference fringes is shown in Fig.2 for the transmission of microwaves through a quarter–wavelength stack of 9 polystyrene plates (index 1.6, thickness 6 mm) spaced by quarter–wavelength air layers. In such a simple one–dimensional layered structure, a very pronounced stop–band or 1–dimensional bandgap occurs around 6.5 GHz. Two curves are present in Fig.2. The heavy curve is a reference interference fringe pattern showing the antenna transmission function when the stack of plates is removed. Variations in the wave envelope as a function of frequency are simply due to variations in the antenna efficiency. The lighter curve represents the experimental signal, the interference fringe pattern observed when the quarter wavelength stack of plates is inserted into the path of the microwave beam. Over a 2GHz band, centered on 6.5 GHz, the transmitted beam is severely attenuated. This is the stop–band.

Notice also the phase shift with respect to the reference beam in Fig.2. At 4.5 GHz and at 9 GHz, on either side of the stop–band, the signal fringes and the

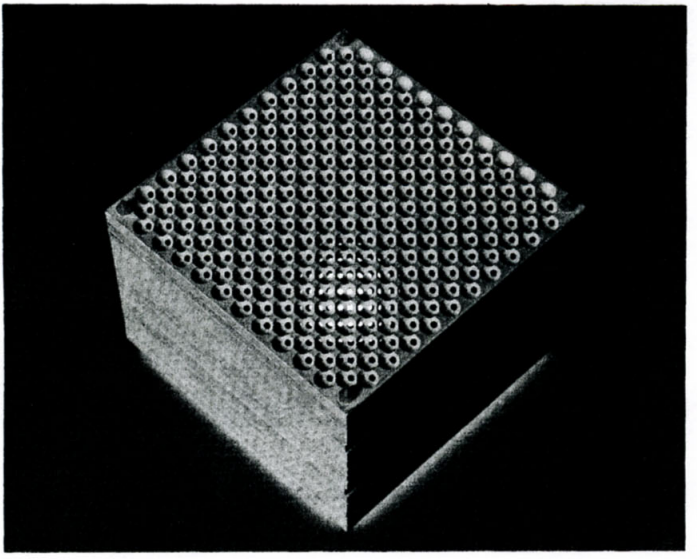

Fig.3 A photograph of the 3–dimensional periodic structure which had a "photonic band gap". This face–centered–cubic crystal consisted of spherical air–atoms which were *larger* than close–packed. The resulting overlap of the air–atoms allows us to see visible light transmitted all the way through along the <111> direction. The spherical air–atoms occupy 86% of the volume. The interstices between the atoms are filled with dielectric material of refractive index 3.5. The overall structure is 86% air and only 14% solid material.

reference fringes are essentially in phase. The opposite effect occurs at the band edges. Due to group velocity dispersion, the signal beam is shifted roughly 180° compared to the reference beam at the upper and lower band–edge frequencies, 5.5 GHz and 7.5 GHz respectively. The relative phase shift is linearly proportional to wave–vector $\boldsymbol{k}$. In principle,with an apparatus of this type, it is possible to map ou the full dispersion relation, i.e. frequency versus wave–vector or ω vs $\boldsymbol{k}$. Similarly, commercial equipment such as the HP–8510 Network Analyzer, can read out directly in terms of group velocity versus frequency.

Our most interesting crystal, exhibited in Fig.3, is the one which has a photonic band gap. Its structure is most unusual. The spherical atoms consist of air, while the space between the atoms is filled with a dielectric material. This commercial low–loss dielectric material, Emerson & Cumming Stycast–12, has a microwave refractive index = 3.5. The volume fraction occupied by the spherical air–atoms is 86%. In fcc close–packed structures, the atomic volume is only 74%. Therefore the atomic spheres in Fig.3 are actually "closer than close–packed", i.e. they overlap slightly. Due to the overlapping atoms, it is possible to see all the way through the crystal along certain directions. The bright spots of light emerging on the top surface of the crystal in Fig.3 are being channeled from below along the <111> direction.

Crystals consisting of spherical air–atoms are relatively easy to fabricate. A series of hemispheres are drilled on one face of a dielectric plate by a numerically controlled machine tool. On the opposite face of the plate an offset series of

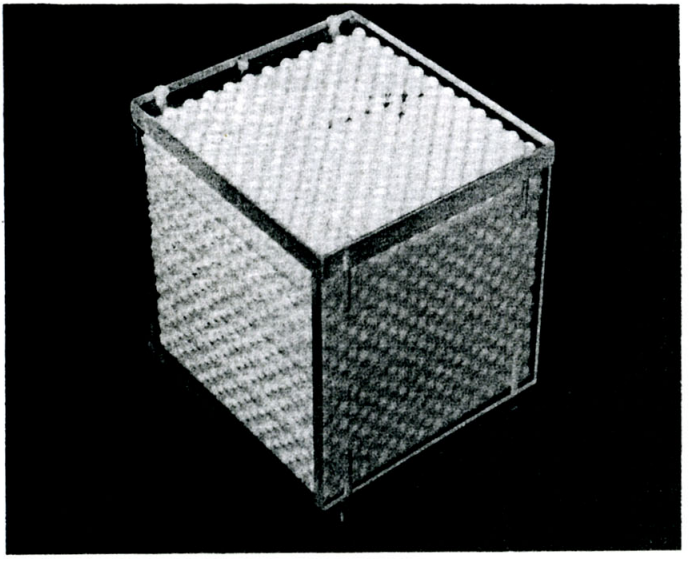

Fig.4 A photograph of a 3–dimensional face–centered–cubic crystal consisting of Al_2O_3 spheres of refractive index 3.06. These dielectric spheres are supported in place by the blue foam material, refractive index 1.01. These spherical dielectric atom structures failed to show a "photonic band gap" at any volume fraction.

hemispheres are drilled. Then many of these plates are simply stacked up so that the hemispheres face one another, forming spherical air–atoms. The volume fraction is varied changing the hemisphere diameter.

The beauty of spherical air–atom crystals is that they are self–supporting. The more obvious fcc structure consisting of dielectric spheres is self–supporting only for the case of close–packing. For any smaller volume packing fraction, the dielectric spheres must be supported in position. The dielectric spheres consisted of polycrystalline Al_2O_3, 6 mm in diameter with a microwave refractive index = 3.06. The volume fraction was varied by changing the sphere spacing. The dielectric spheres were supported by thermal compression molded dielectric foam of refractive index ~ 1.01. Precision molds were built of Aluminum jig plates having 6 mm diameter steel ball bearings embedded in them. Dielectric foam pads were molded at 95°C, with the molds released at 40°C. The hemispherical depressions in the molded foam were then filled with the Al_2O_3 spheres and the structure built up into many layers. Fig.4 is a photograph of such a crystal consisting of dielectric spheres supported by the blue dielectric foam.

The philosophy behind our experiments is to map out the frequency versus wave vector dispersion relations for a whole series of 3–dimensional fcc crystals. For each crystal it becomes necessary to explore all the different angles in reciprocal space. The interference fringe pattern in Fig. 5 is an example of such a measurement on the 86% spherical air–atom crystal of Fig.3. These fringes are produced in the homodyne detection system by an electromagnetic wave propagating toward the L–U line of the hexagonal L–plane in reciprocal space. This wave was predominantly s–polarized, i.e. it was polarized parallel to the X–plane. Two important items emerge from Fig.5. The lower gap edge frequency and the upper gap edge frequency. The lower edge was defined by the sudden drop in microwave transmission relative to a reference scan with the crystal absent. The upper edge is defined by the frequency at which the transmitted signal recovers.

These two frequencies define band edges, but these band edges do not necessarily fall at exactly the same point on the surface of the Brillouin Zone. The reciprocal space position of these frequency edges is determined by momentum conservation between the external and internal electromagnetic waves. In our experiments, the incoming plane wave was generally incident on the <100> face of the crystal. (The <100> face is by definition perpendicular to the <100> momentum direction.) Upon transmission through the crystal surface, only the component of wave vector momentum parallel to the surface plane is conserved. This is very similar to the principle which leads to Snel's Law. In our geometry it means that component of wave vector momentum perpendicular to the <100> direction, $<0,k_y,k_z>$ is conserved upon entering the crystal. The position of the frequency edge in reciprocal space is the point on the Brillouin Zone surface having those identical momentum components k_y and k_z. In our experiments, the external angle of incidence is held fixed as the frequency is swept. Therefore the upper and lower gap edge frequencies will have different k_y,k_z and different Brillouin Zone positions.

Due to the limitations on the external wave vector $<0,k_y,k_z>$ which could be attained in air, some parts of the internal Brillouin Zone sometimes had to be accessed by transmission through a pair of giant microwave prisms on either side of the crystal. The prisms, over 15 cm square, were made of polymethylmethacrylate (microwave refractive index 1.6) to increase the available external wave vector.

Step by step, the angle of incidence is varied, and the frequency of the first and second band edges is mapped out on the surface of the Brillouin Zone. Our

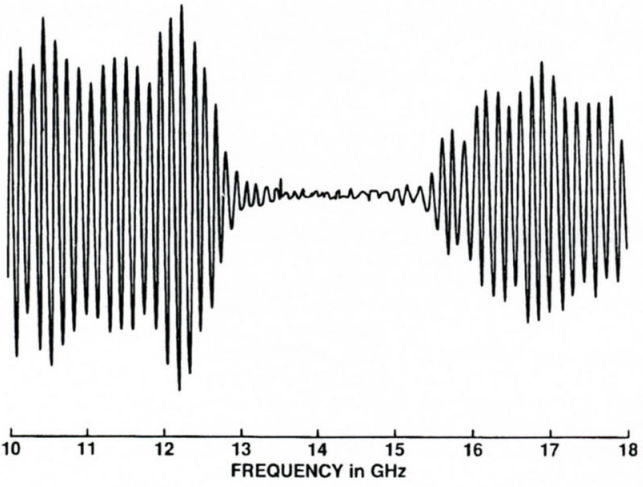

Fig.5 The forbidden gap observed on the crystal displayed in Fig.3 measured along the L–U line of the L–plane. The electromagnetic wave is polarized parallel to the X–plane (s–polarization).

measurements concentrated on the high symmetry planes X–U–L and X–W–K, though lower symmetry points were also occasionally investigated. (See Fig.6 for a description of the Brillouin Zone point labels). Unfortunately, with this method it is not possible to learn much about the higher frequency bands above the two lowest band edges. At higher frequencies, a superposition of allowed electromagnetic modes can become excited by an incident plane wave. This makes it very difficult to disentangle any higher band edges. Accordingly, we determine only the first gap edge where transmission is cut off and the second where transmission cuts on again. In keeping with the electron band structure analogy, the first gap edge may be called the valence band and the second gap edge may be called the conduction band.

The result of these measurements on our 86% spherical air–atom fcc dielectric structure (photographed in Fig.3) is plotted in Fig.6. For electromagnetic waves, two band structures must be shown, allowing for the two different polarization states of electromagnetic waves. The forbidden bandgap in Fig.6 is filled in by slanted lines. The lines that are slanted to the right fill in the bandgap for linear polarization parallel to the X–plane, (mostly s–polarized). The left slanted lines fill in the bandgap for the orthogonal linear polarization with a partial component perpendicular to the X–plane, (mostly p–polarized). On the high symmetry planes X–U–L and X–W–K, the two linear polarizations are not expected to mix, and therefore the linearly polarized antenna excites electromagnetic eigenstates of the crystal. Off the high symmetry planes, the polarization eigenstates are no doubt complex, and some type of elliptical polarization should be expected. No absolute frequency units are given on Fig.6, since the frequencies should all scale with the

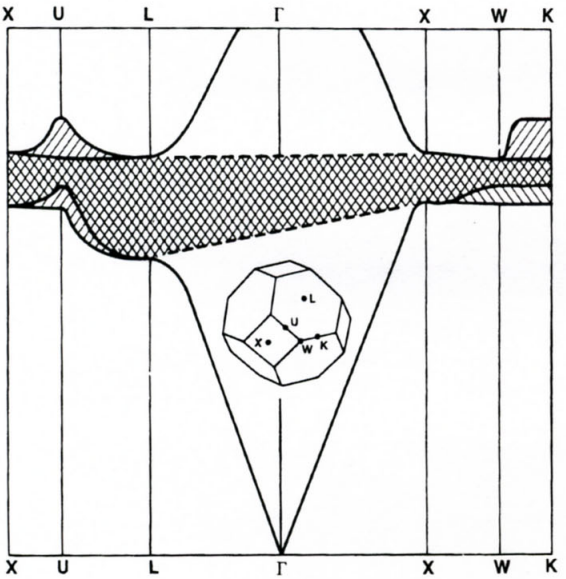

Fig.6 The experimentally observed photonic band structure in reciprocal space of the face–centered–cubic "spherical air–atoms" surrounded by the dielectric configuration of Fig.3. The right sloping lines represent polarization parallel to the X–plane, while the left sloping lines represent the orthogonal polarization which has a partial component out of the X–plane. The cross hatched region where both polarizations are forbidden in all directions in k–space is the "photonic band gap".

reciprocal linear size of the crystal spacing. On the actual crystal, the fcc unit cube length "a" was equal to 12.7 mm and the forbidden gap was ~ 1 GHz wide, centered at 15 GHz.

The band structure in Fig.6 plots frequency versus real wave vector. At frequencies within the forbidden gap, the wave vector is pure imaginary, and it measures the attenuation length within the crystal. Attenuation was generally very strong within the bandgap, consistent with a 1/e attenuation length of only one or two crystal unit cells. At points where the bandgap was very narrow, however, particularly for p–polarized waves at the point U, the attenuation length was much longer, ~ 10 or 20 unit cells.

All the other crystal structures that were fabricated and tested in our experiments produced "semi–metals" rather than "photonic band gaps". Most frequently, the conduction band at the point L in the Brillouin Zone generally tended to overlap in energy with the valence band at the points W and U. An example of such a band structure is shown in Fig.7 for the case of 50% volume fraction spherical air–atoms embedded in polystyrene of refractive index 1.6. In our experiments we found that it was essential to start out with large forbidden gaps at the points X and L at centers of the square and hexagonal facets of the Brillouin

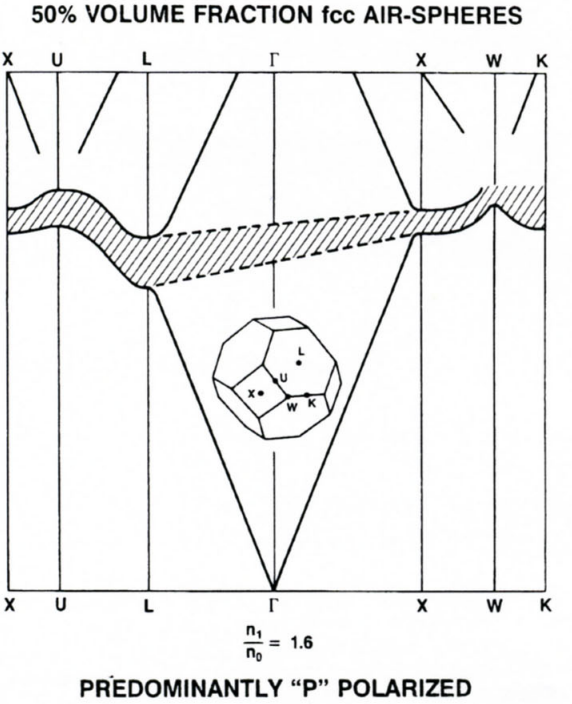

Fig.7 An example of a photonic band structure similar to that of a semi–metal. The fcc structure was 50% volume fraction air–atoms but was made of polystyrene, refractive index only 1.6. The conduction ban at the L–point overlaps the valence band at the U and W points. In order to get a bandgap, both the volume fraction of atoms must be increased and the index contrast must be increased.

Zone. Invariably if bandgaps at the X and L points were inadequate, band overlap would become established at peripheral points between facets, such as U, W, or K In our experimental survey, a semi–metallic band structure occurred in all cases but one.

Let us now analyze more of the band structure properties as a function of volume fraction and structure type. Fig.8 gives the index of refraction of the different crystal structures as a function of volume filling fraction. The effective refractive index is defined as $c/a\nu_X$, in terms of the center frequency, ν_X, of the X–point gap. We found that the X–point center frequency was a good extrapolation of the low frequency dispersion out to the X–point. Therefore $c/a\nu_X$ is a good surrogate representation of the long wavelength refractive index of the composite structure represented by these fcc crystals. For both the spherical

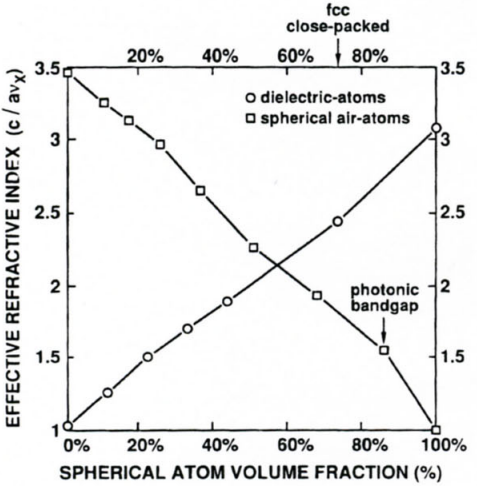

Fig.8 The effective long wavelength refractive index, $c/a\nu_X$, measured on two basic crystal structures of various volume fractions where c is the speed of light in vacuum, a is the length of the unit cube, and ν_X is the center frequency of the X–gap. Spherical dielectric atoms are represented by (□)–points and spherical air–atoms are represented by (o)–points. Fcc close–packing occurs at 74% volume fraction. Of all these structures, only the one marked "photonic bandgap" had a forbidden frequency band at all directions in reciprocal space.

air–atoms and the dielectric sphere atoms, a simple linear interpolation of refractive index with volume fraction seems to describe the experimental indices in Fig. 8. Neither of the effective medium theories, not Maxwell–Garnett nor Bruggeman were any more accurate in modelling Fig.8. Only the one structure marked "photonic bandgap" on Fig.8 had a forbidden gap all the way around the Brillouin Zone. All the others were semi–metals as mentioned earlier.

In view of the importance of having large gap widths at the L–point and at the X–point, we present those results in Fig.9. The measured gap width normalized to ν_X is plotted against spherical air–atom volume fraction. All the results in Fig.9 were taken on Emerson & Cumming Stycast–12, a material with index contrast 3.5 to 1 relative to air. It is clear from Fig.9 why the 86% volume fraction spherical air–atom structure has an overall photonic bandgap. Its gap widths are far larger than any of the others. Notice the unusual behavior of the X–gap as a function of spherical air–atom volume fraction. At around 68% volume fraction, the X–gap width becomes undetectable while at the higher volume fraction of 86% it rises again to a very large value. While our measurements can only assign a positive number to the gap width, we have elected to plot this last data point as a negative quantity. As shown in Ref. 2, the gap width on any plane in reciprocal space is proportional to the corresponding Fourier component of the dielectric constant. We

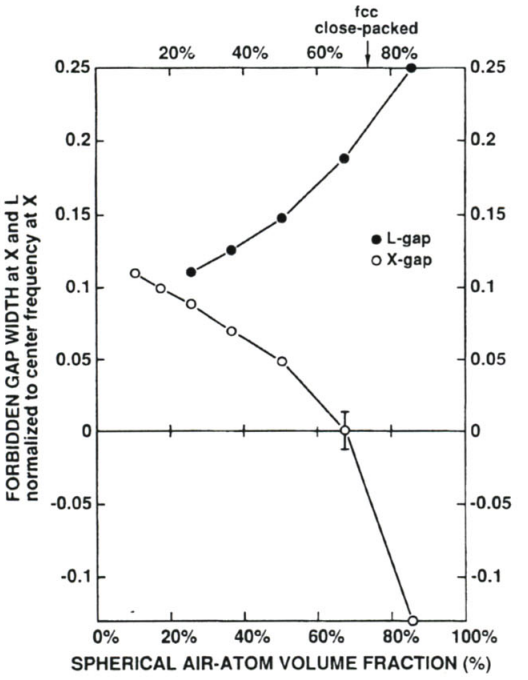

Fig.9 The forbidden gap width normalized to ν_X observed at the L–point (●), and at the X–point (○) for a series of spherical air–atom fcc crystals of varying atomic volume fraction. The dielectric material between air–atoms had a refractive index of 3.5. We have elected to plot the 86[X–point gap width as a negative number since the <200> Fourier component has opposite sign on either side of the null point at 68% volume fraction.

believe that the zero gap at 68% volume fraction is a node at which the Fourier component of dielectric modulation changes sign.

For the X–plane Fourier component of the dielectric constant to change sign a a volume fraction around close packing is not entirely surprising. Fig.10 is a perspective view of the fcc close–packed structure. Remember that the spheres ar air and the spaces between the spheres are filled with dielectric material. At the lower edge of the bandgap, the Bloch electric wave function tends to be concentrated in the high dielectric constant layers, while the upper edge electric field function tends to concentrate in the low dielectric constant layers. For the sake of definiteness let us concentrate on lower edge or valence band electric field function near the X–plane. The electric field will seek out those layers parallel to the cube faces in Fig.10 which have the highest dielectric constant. If the spherica air–atoms are much smaller than close–packed, the electric field will weave

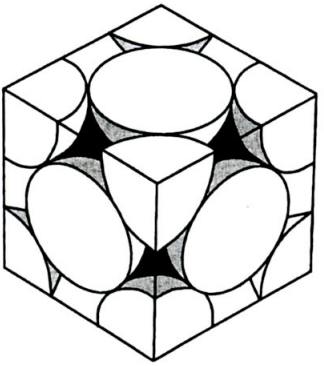

Fig.10 A close–packed face–centered–cubic structure. If the atoms are air–filled and smaller than close–packed, the electric field lines of the valence band edge X–gap mode will tend to weave between atomic layers. If the air–atoms are larger than close–packed, or if they are filled with dielectric material, the electric field lines of the valence band edge X–gap mode will tend to concentrate within the planes of atoms.

between the layers of atoms and avoid the atomic layers themselves. For spherical air–atoms larger than close–packed, as can be seen from Figs.10 and 3, there is little dielectric material left between the atomic layers and most of the remaining material is in the cusp shaped volumes in the planes of atoms. In that case the electric field tends to concentrate in the atomic layers themselves.

The plane containing the most dielectric material shifts from the inter–atomic layers to the atomic layers as the spherical air–atom volume fraction goes up. As a consequence, the amplitude of the Fourier component of the dielectric constant goes through zero and changes sign. This explains the peculiar behavior of the X–gap width in Fig.9, and justifies plotting the 86% data point as a negative quantity. In that last case the valence band Bloch electric wave function tends to concentrate in the planes of atoms along the cube faces.

By inspection of Figs.3 and 10, it is clear that there is no tendency for the L–plane dielectric Fourier component to change sign. The electric field tends to concentrate between the layers of atoms and there is no indication of a node in the data. Therefore the L–gaps were all plotted as positive quantities.

The gap widths for spherical dielectric Al_3O_2 atoms are displayed in Fig.11. The gap widths are all rather feeble, explaining why no overall photonic band gap was observed for dielectric spheres. The L–plane gap was particularly weak. It exhibited a polarization dependence even at the center of the hexagonal L–plane, where s and p polarization are degenerate. The X–plane gap was stronger. There were some indications that the 74% volume fraction X–gap data point should have been plotted as a negative quantity as before. That data point was unusually sensitive to tiny changes in packing geometry, possibly indicating that it was near a node. In the absence of any additional information, we simply left the 74% X–gap width as a positive number in Fig.11. The index contrast in this case was

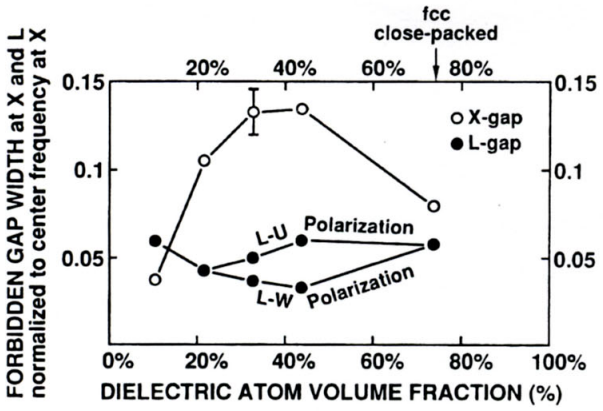

Fig.11 The forbidden gap width normalized to ν_X observed at the L–point (●), and at the X–point (○) for a series of fcc crystals made of Al_2O_3 spherical dielectric atoms, (refractive index 3.06). The atomic volume fraction was varied by changing the size of the unit cube. Overall, the L–point gap width was too feeble for the existence of a "photonic band gap".

3.03 to 1, somewhat less than the spherical air–atom case. But that is not the reason for the absence of a photonic band gap for the Al_3O_2 dielectric spheres. Instead the absence must be attributed to the smallness of the L–plane gap at all tested volume fractions.

3. THEORY

A starting point for the behavior of light waves in 3–dimensionally periodic dielectric structures is derived from Maxwell's equations

$$-\nabla^2 E + \nabla(\nabla \cdot E) = \epsilon(\boldsymbol{x}) \frac{\omega^2}{c^2} E, \tag{1}$$

where E is the optical electric field, c the speed of light, ω is the optical frequency, which plays the role of an eigenvalue, and the geometry of the dielectric structure is contained in the spatial dependence of dielectric constant $\epsilon(\boldsymbol{x})$. The dielectric constant is related to the refractive index by $\epsilon \equiv n^2$. Eq. (1) resembles Schrödinger's equation if $\epsilon(\boldsymbol{x})\omega^2/c^2$ is identified with the kinetic energy term $2m[E - V(\boldsymbol{x})]/\hbar^2$, where m is the electron mass, $\hbar$ is Planck's constant divided by 2π, E is the total energy eigenvalue and $V(\boldsymbol{x})$ is the potential energy.

In optics we are generally restricting ourselves to positive dielectric constant materials. Metals, which have negative dielectric constants, invariably have significant dissipation as well, i.e. an imaginary component to $\epsilon(\boldsymbol{x})$. Among the high quality optical materials, particularly semiconductors, a high positive

dielectric constant in the transparent region is accompanied by virtually no dissipation. This means that the kinetic energy term $\epsilon(x)\omega^2/c^2$ must always be positive in non–dissipative dielectric structures. If potential barriers are allowed, in which the kinetic energy is negative, it would be much easier to confine the wave functions, to produce localization, and to produce forbidden bandgaps. In optics with positive dielectric constant, it is very challenging to create a photonic band gap. For electrons, in a tight binding model for example, a forbidden bandgap occurs right from the outset. This is the main reason why only one dielectric crystal, out of the many we tested, had a photonic band gap.

As shown in Ref.2, the vector character of (1) also contributes to the difficulties of creating a photonic band gap. Waves which are p–polarized relative to the local Brillouin Zone surface interact more weakly. Vector wave equations are extremely difficult to solve [5]. This is a pity, since for solid state band theorists, our dielectric structures represent the classic muffin–tin–potential. In the scalar wave case, this famous potential would be soluble. The various methods for solving wave equations in 3–D periodic media are reviewed in Chapter 9–11 of Ashcroft & Mermin [6]. In view of the relatively small gap widths we have found experimentally, and the difficulty of adapting some of the more sophisticated band theory methods to vector waves, we will analyze our data in terms of the "nearly free photon model". This is analogous to the well–known "nearly free electron model", and is appropriate so long as the wave functions are weakly perturbed plane waves. The widest relative gap width, which measures the strength of perturbation, occurred at the L–point in the 86% spherical air–atom crystal and was only $\sim 1/4$. All other gap widths in all the crystals were at least a factor 2 smaller, lending reasonable credence to the "nearly free photon model".

The "nearly free photon model" predicts a splitting of bands at the Brillouin Zone surfaces

$$\omega_{\pm} = \omega_0 \left[1 \pm \frac{n_G}{n_0}\right], \tag{2}$$

where $\omega_{\pm}$ are the angular frequencies of the upper and lower band edges and ω_0 is the center frequency at that point on the Brillouin Zone surface, n_G is the Fourier component of the refractive index corresponding to the reciprocal lattice vector G defining that face of the Brillouin Zone and n_0 is the mean refractive index. For the case of a layered structure with refractive index contrast Δn between layers, the corresponding $n_G = \Delta n/\pi$. In three–dimensional structures, the refractive index contrast is not organized into simple layers, and the plane wave Fourier components n_G tend to be much weaker than $1/\pi$ times the index contrast Δn.

Eq.(2), as written, applies only to s–polarized electromagnetic waves with respect to the Bragg reflection planes on the Brillouin Zone surface. For p–polarized waves, the scattering efficiency is diminished by the projection of the polarization vector onto the new scattered direction. Accordingly, n_G is diminished by $\cos(2\theta) = 2\cos^2\theta - 1$, where θ is the angle of incidence onto the Bragg plane forming the Brillouin Zone surface. The largest angle in the fcc structure is $\theta = 39°$, subtended by the points L and W. In Yeh [7] the forbidden gap width is increased by a further angle dependent factor, $1/\cos^2\theta$. The reason for this additional factor is that they are considering the stop–band for a fixed angle of incidence. As explained earlier in the experimental section of this paper, the component of photon momentum parallel to the entry plane is conserved. Therefore the upper and lower band edge frequencies observed experimentally, appear at *different* points along the Brillouin Zone surface. The apparent gap

width becomes larger by $1/\cos^2\theta$. By contrast, (2) gives the band edge frequencies and gap width at a *single* point on the Brillouin Zone surface.

The quantity n_G/n_0 plays the role of a dimensionless pseudo–potential in the "nearly free photon model" and we will give it the label V_G. For example, the pseudopotential corresponding to the $G = <111>$ on the hexagonal L–plane of the Brillouin Zone can be defined $V_1 \equiv n(<111>)/n_0$. The dimensionless pseudo–potential corresponding to the $G = <200>$ on the square X–plane of the Brillouin Zone can be defined $V_2 \equiv n(<200>)/n_0$. In general these pseudo–potentials can also be expected to depend on polarization angles as explained above.

The "nearly free photon model" becomes particularly interesting at points of degeneracy on the Brillouin Zone surface. For example, at the point W, four different plane waves are degenerate and they mix to produce eigenmodes which break the degeneracy. Similarly at the point U, three different plane waves mix to produce a superposition of plane waves. As shown in Ref.6, the solution requires the diagonalization of the following matrix

$$\begin{bmatrix} -\Delta\omega/\omega_W & V_1 & V_1 & V_2 \\ V_1 & -\Delta\omega/\omega_W & V_2 & V_1 \\ V_1 & V_2 & -\Delta\omega/\omega_W & V_1 \\ V_2 & V_1 & V_1 & -\Delta\omega/\omega_W \end{bmatrix} = 0, \tag{3}$$

where ω_W is the center frequency at point W in the Brillouin Zone and $\Delta\omega \equiv (\omega - \omega_W)$ where ω are the new eigenfrequencies. The solutions to (3) are as follows

$$\Delta\omega/\omega_W = -V_2 \quad \text{(twice)}, \tag{4a}$$

$$\Delta\omega/\omega_W = V_2 \pm 2V_1. \tag{4b}$$

Of these four solutions, the two in (4a) are degenerate. This degeneracy is no accident, nor is it specific to the "nearly free photon model". It is quite general and arises directly from the group–theoretical properties of the W–point in the fcc structure. In the character tables given by Callaway [8], the W_3 representation is doubly degenerate. If solution (4a) were to be the lowest lying frequency at the point W, then a photonic band gap would be impossible, since valence and conduction bands would touch. This can be prevented in two ways: (i) V_1 can be larger than V_2. (ii) As shown in Fig.9, V_2 can be negative. Either case will ensure that at least one of the two solutions (4b) is below solution (4a).

The difference between the wave functions for solutions (4a) and (4b) can be visualized from Fig.10. The mixing of the plane waves along the cubic X–axis results in standing waves which peak either within the plane of atoms on the cubic face or between the planes of atoms. Depending upon whether the atoms are made up of air or dielectric spheres, one of these standing waves will be bonding (lower in frequency) and the other will be anti–bonding (higher in frequency). The <200> standing wave peaking on the cubic face will, at the W–point, interact strongly with other standing waves in the <111> directions, leading to solution (4b). For the other <200> standing wave, having nodes on the fcc cube faces, the interaction with <111> plane waves cancels out, leading to (4a).

Similarly, the matrix equation for the point U is

$$\begin{bmatrix} -\Delta\omega/\omega_U & V_1 & V_2 \\ V_1 & -\Delta\omega/\omega_W & V_1 \\ V_2 & V_1 & -\Delta\omega/\omega_U \end{bmatrix} = 0, \tag{5}$$

where ω_U is the center frequency at point U in the Brillouin Zone and $\Delta\omega \equiv (\omega - \omega_U)$. The solutions to (5) are as follows

$$\Delta\omega/\omega_U = -V_2/2, \tag{6a}$$

$$\Delta\omega/\omega_U = V_2/2 \pm [(V_2/2)^2 + 2(V_1)^2]^{1/2}. \tag{6b}$$

For solution (6a), as before, the effect of the <111> pseudo–potential cancels out.

We are now in a position to test (4) and (6) against the observed band structure at the points W and U in Fig.6. It is necessary to take polarization into account. Fortunately, as discussed earlier, in the high symmetry planes X–U–L and X–W–K, there exist two orthogonal linear polarization which are not expected to mix. At the U–point these divide neatly into s–polarized parallel to the X–plane and *p*–polarized parallel to the X–U–L plane. At the W–point the two polarizations are not purely *s* or *p*, but they are orthogonal nevertheless. One polarization is parallel to the X–W–K plane and the other is parallel to the X–plane. Each orthogonal polarization leads to its own matrix equation, (3) or (5), with its own values of V_1 and V_2 which must be adjusted by polarization angle dependent factors. For *p*–polarization at the U–point, V_2 is multiplied by $\cos(2\theta) = 7/9$ and V_1 is multiplied by $\cos(2\theta) = 1/3$. Substituting into (6), the calculations are in reasonable agreement with experiment for both polarization components of the measured band structure at the point U in Fig.6.

A similar calculation (requiring more trigonometry) at the W point leads to gap widths that are significantly larger than observed in Fig.6. We do not know the reason. Evidently, we may possibly have reached the limits of the "nearly free photon model" at the W point.

4. CONCLUSIONS

We have found that the idea of a "photonic band gap" can be experimentally realized in 3–dimensionally modulated dielectric structures. It required a refractive index contrast approaching 3.5 to 1 and the optimal structure consisted of 86% spherical air–atoms and only 14% dielectric material. All the other structures that we tested were "semi–metals" with the conduction band minimum at the L–point overlapping with the valence band maximum at the W or U point. In particular, this included all the tested structures consisting of spherical dielectric atoms.

The main reason for the difficulty in producing a photonic band gap was that the Fourier components of the index modulation in a 3–dimensional structure tend to be much weaker than in a simple 1–dimensional layered structure. In the spherical dielectric atom case the <111> Fourier components tended to be particularly weak. It should be possible to scale the optimal structure from microwave wavelengths down to the near–infrared by microfabrication in semiconductors like Silicon and GaAs which do possess the required refractive index.

We would like to thank Prof. S. John for numerous discussions and Prof. Gene Mele for advice regarding the group theory.

REFERENCES

[1] E. Yablonovitch, Phys. Rev. Lett. 58 (1987) 2059.
[2] S. John, Phys. Rev. Lett. 58 (1987) 2486.
[3] S. John, Comm. Cond. Matt. Phys. 14 (1988) 193.
[4] G. Kurizki and A.Z. Genack, Phys. Rev. Lett. 61 (1988) 2269.
[5] S. John and R. Rangarajan, Phys. Rev. B38 (1988) 10101.
[6] N.W. Ashcroft and N.D. Mermin, *Solid State Physics* (W.B. Saunders, Philadelphia, 1976).
[7] P. Yeh, *Optical Waves in Layered Media* (Wiley, N.Y., 1988) 36.
[8] J. Callaway, *Quantum Theory of the Solid State*, Part A (Academic Press, New York, 1974) Appendix C.

E. Yablonovitch is with Bell Communications Research, Navesink Research Cent
Red Bank, N.J. 07701–7040, USA.